

## Article

# Deterioration of White Tempera Mock-Ups Paints in a SO<sub>2</sub>-Rich Atmosphere

Teresa Rivas <sup>1</sup>, José Santiago Pozo-Antonio <sup>1,\*</sup>, Daniel Jiménez-Desmond <sup>1</sup>, Amelia Dionísio <sup>2</sup> and Carolina Cardell <sup>3</sup>

<sup>1</sup> CINTECX, GESSMin Group, Dpto. de Enxeñaría de Recursos Naturais e Medio Ambiente, Universidade de Vigo, 36310 Vigo, Spain; trivas@uvigo.gal (T.R.); danieljose.jimenez@uvigo.gal (D.J.-D.)

<sup>2</sup> CERENA, Instituto Superior Técnico, Universidade de Lisboa, 1049-001 Lisboa, Portugal; amelia.dionisio@ist.utl.pt

<sup>3</sup> Department of Mineralogy and Petrology, Faculty of Science, University of Granada, 18071 Granada, Spain; cardell@ugr.es

\* Correspondence: ipozo@uvigo.gal

**Abstract:** Historical tempera paints exposed to pollutant gases suffer chemical and mineralogical deterioration which manifests through physical changes. Knowledge about these changes is fundamental to develop strategies for preventive conservation of wall paintings. In this research, binary tempera mock-ups composed of calcite, gypsum or lead white mixed with a proteinaceous binder (i.e., egg yolk or rabbit glue) were exposed to an aging test by using SO<sub>2</sub>-rich atmosphere exposure to learn about the degradation mechanisms and forms related to the pigment–binder interaction. Reference (unaltered) and aged mock-ups were studied from a physical point of view, characterizing the morphological changes by using stereomicroscopy and profilometry, color variations by using spectrophotometry, gloss changes, and reflectance changes by using a hyperspectral camera. Also, mineralogical and chemical changes were studied by means of X-ray diffraction, Fourier transform infrared spectroscopy and scanning electron microscopy with energy-dispersive X-ray spectroscopy. Egg-yolk-based paints showed higher chromatic changes than their counterparts made of rabbit glue binder. Also, sulfate and sulfite salts precipitated on the surface of the aged paints regardless of their binder, influencing the painting reflectance which subsequently increased. Egg-yolk-based mock-ups exhibited roughness increases while the rabbit-glue-based paints showed roughness reduction, with the exception of lead-white-based paints. Therefore, the important influence of the type of binder and the interaction between the binder and the pigment on the durability of tempera paints in atmospheres rich in SO<sub>2</sub> was confirmed.



Academic Editor: Asterios Bakolas

Received: 14 December 2024

Revised: 26 January 2025

Accepted: 2 February 2025

Published: 5 February 2025

**Citation:** Rivas, T.; Pozo-Antonio, J.S.; Jiménez-Desmond, D.; Dionísio, A.; Cardell, C. Deterioration of White Tempera Mock-Ups Paints in a SO<sub>2</sub>-Rich Atmosphere. *Appl. Sci.* **2025**, *15*, 1610. <https://doi.org/10.3390/app15031610>

**Copyright:** © 2025 by the authors. Licensee MDPI, Basel, Switzerland. This article is an open access article distributed under the terms and conditions of the Creative Commons Attribution (CC BY) license (<https://creativecommons.org/licenses/by/4.0/>).

**Keywords:** wall paintings; preventive conservation; tempera painting; calcite; Bianco di San Giovanni; gypsum; lead white; binder

## 1. Introduction

Over the last decades, part of the research studies carried out in the field of the conservation of cultural heritage has been focused on studying the influence of atmospheric contamination on the construction materials used in architectural heritage [1–3]. Monuments and historical buildings are frequently located in urban environments where air contamination coming from traffic, industrial and construction activities and domestic heating have negative consequences on the materials used in structures and decorative elements. It is known that, among cultural heritage materials, outdoor historical wall

paintings are also sensitive to anthropogenic pollutants, suffering, consequently, deterioration and subsequent loss [4]. Hence, it is important to characterize the decay forms and clarify the degradation mechanisms of such historical paintings when exposed to contaminated atmospheres in order to develop respectful conservation and restoration strategies [5,6].

Even though SO<sub>2</sub> levels have been reduced over the last decades [7], sulfur dioxide continues to be the main pollutant gas involved in the deterioration of building stones [5] and the main agent responsible for the sulfation process of historical paintings [6,8]. In this respect, the high porosity of the paint layers and their underlying mortars are susceptible to pollution-induced chemical decay. This deterioration also involves the action of particulate pollutants, as well as other atmospheric factors, such as moisture [1,2].

Tempera is an old painting technique that consists of an emulsion where pigments are mixed with a water-soluble binder, typically of a proteinaceous nature, such as egg yolk, rabbit glue, casein (milk) or gums [9]. The tempera technique was replaced by oil painting in the Late Renaissance and Baroque periods; however, a remarkable revival of the tempera technique has taken place since the 20th century [10]. Tempera wall paintings are widely spread along the south of Spain following the so-called a secco technique where, unlike in the buon fresco technique, pigments are fixed to the surface mixed with an organic binder [4,10]. Tempera paintings are long-lasting since good examples from the ancient Egyptian period still stand [11]. Since the substrate in contact with water is a significant source of Ca<sup>2+</sup> and CO<sub>3</sub><sup>2-</sup> ions, in contaminated atmospheres, oxides, sulfates, sulfites, oxalates, carboxylates and carbonates are commonly found as degradation forms of tempera paint materials [4,6,12–16]. Gypsum (CaSO<sub>4</sub>·2H<sub>2</sub>O) has been identified in wall paintings [12], in lime-rich mortars (i.e., made of calcite, CaCO<sub>3</sub>) exposed to medium/high SO<sub>2</sub> levels in south Italy [4], and in lime-based tempera mock-ups artificially aged in SO<sub>2</sub> rich atmospheres in the presence of moisture [6]. In the case of lead white (2PbCO<sub>3</sub>·Pb(OH)<sub>2</sub>), a pigment very susceptible to saponification by reaction with oil binders [14], blackening occurs when it is present in fresco paintings and subjected to SO<sub>2</sub> exposure. This is due to the formation of (i) PbO<sub>2</sub>, due to the interaction with oxidizing agents, ii) or to the formation of PbS [15]. The exposure of paintings made with this pigment to sulfur pollutants and humidity results in the formation of Pb sulfides and Pb sulfates [16].

All these degradation products trigger colorimetric changes that can be increased by chemical modifications promoted by the interaction of the paint components with sunlight and atmospheric pollutants, as well as by physical changes that take place mostly due to pigment–binder interactions [17]. Regarding this interaction, recent studies have shown that the susceptibility to deterioration due to exposure to a SO<sub>2</sub> atmosphere depends greatly on the type of binder and its interaction with the pigment. Firstly, it seems that the susceptibility to deterioration of the binder varies depending on its composition. For instance, it was observed that egg-yolk-based mock-ups were more stable than rabbit-glue-based paints [18,19]. Indeed, SO<sub>2</sub>-exposed egg-yolk-based paint mock-ups prepared with blue and green pigments, i.e., azurite, malachite, blue smalt and lapis lazuli [18,19], remained physically intact, although sulfate salts precipitated on their surfaces. In addition, a yellowing of the binder was also noticed. Conversely, the corresponding rabbit glue-based paint mock-ups developed intense cracking and binder loss, and sulfated salts were present in lesser amounts. Secondly, in these works, it was found that the effects of the deterioration of the binder depended on the pigment with which it was mixed. All these studies are focused on blue and green pigments (some of them of carbonate nature) but not white pigments, which also suffer serious degradations that lead to color changes and a loss of stability. Therefore, it is necessary to undertake a

specific study on the behavior of these white pigments during the same deterioration test of these previous works, which will allow us to know the susceptibility of these pigments to SO<sub>2</sub> exposure and, in the case of carbonates, to compare their behaviour with that of other colored carbonates, such as malachite or azurite. This paper gathers information on the stability of binary tempera paint mock-ups made of a proteinaceous binder (egg yolk or rabbit glue) mixed with a white pigment, more precisely with calcite, also named Bianco San Giovanni (CaCO<sub>3</sub>), white lead (2PbCO<sub>3</sub>·Pb(OH)<sub>2</sub>) and gypsum (CaSO<sub>4</sub>·2H<sub>2</sub>O) under exposure to SO<sub>2</sub> atmospheric conditions in a climatic chamber. Reference (unaltered) and artificially aged mock-ups were studied from a physical point of view, characterizing textural changes under a stereomicroscope and by means of profilometry, color changes using a spectrophotometer, gloss changes by using a glossmeter and reflectance changes using a hyperspectral camera. Also, mineralogical and chemical changes after SO<sub>2</sub> exposure were studied by using X-ray diffraction (XRD), Fourier transform infrared spectroscopy (FTIR) and scanning electron microscopy with energy-dispersive X-ray spectroscopy (SEM-EDS). The results presented here are part of an ongoing investigation which aims to address the effect of the SO<sub>2</sub> pollutant on the physical–chemical stability of tempera paints considering the pigment–binder interaction, as well as the pigment grain size [18,19].

## 2. Materials and Methods

### 2.1. Materials

In this study, fourteen tempera mock-ups were studied made with a mixture of one inorganic pigment, namely calcite (CA), gypsum (G) or lead white (LW) and a proteinaceous binder (egg yolk or rabbit glue). In the case of the calcite and gypsum pigments, several commercial granulometries were used to prepare the temperas (Table 1): extra-fine (EF), fine (F), standard (ST), medium (M) and coarse (C). Traditionally, gypsum was mixed with other pigments in paint layers or used as white ground in, e.g., wall paintings [9]. Calcite was usually used as a filler pigment in paint layers, either to reduce cost or to add bulk and consistency to paint layers when combined with other pigments [9]. Lead white is a pigment widely used since ancient times until the end of the 19th century, both in grounds and in paint layers, due to its dense opacity and bright shade. The pigments were supplied by Kremer Pigments GmbH & Co. KG (Aichstetten, Germany) (Table 1). Two proteinaceous binders were used: pearls of rabbit glue (collagen, ref. 63028) from Kremer Pigments GmbH & Co. KG (Aichstetten, Germany) and egg yolk (albumin, ovalbumin and fatty acids) from commercial eggs from the area.

Paint mock-ups were prepared according to Old Master recipes [20]. The procedure followed to prepare the paints can be consulted in [17,18]. The obtained paints were then applied by brush onto glass slides (ca. 75 mm × 25 mm × 1 mm) in several successive layers, waiting for the previous layer to dry completely after each application. Tempera mock-ups were identified by adding to the pigment code the letter denoting the type of binder (E-egg yolk; R-rabbit glue). Table 1 shows the commercial name, identification code, mineral composition and grain size of the pigments reported by the manufacturer, and the mineralogy, grain size and identification code of the paint mock-ups according to the authors. Next, each paint mock-up was cut in two pieces: one part to be used in the SO<sub>2</sub> exposure aging test and the other part to be kept as the reference (unaltered) paint sample. Before starting the aging test, the samples were kept under laboratory-controlled conditions (18 ± 5 °C; 60 ± 10% RH) for 1 month.

**Table 1.** Properties of the white pigments and tempera paint mock-ups used in this study according to Kremer manufacturer and the authors.

Kremer Pigment Reference	Authors' Identification Code	Kremer Mineralogical Composition	Authors' Mineralogical Composition	Kremer Grain Size ( $\mu\text{m}$ )	Authors' Grain Size ( $\mu\text{m}$ ) *	Mineralogical Composition of Paints Before the Aging Test		Mineralogical Composition of Paints After the Aging Test	
						Egg Yolk Mock-Ups	Rabbit Glue Mock-Ups	Egg Yolk Mock-Ups	Rabbit Glue Mock-Ups
Calcite 58720	CA-EF	Calcite	Calcite Dolomite	20	25 (0.25–100)	Calcite Dolomite	Calcite Portlandite	Calcite Dolomite $\text{Ca}_3(\text{SO}_3)_2\text{SO}_4 \cdot 2\text{H}_2\text{O}$	Calcite Gypsum
<i>Bianco San Giovanni</i> 11415	BSG-ST	Portlandite Calcite	Portlandite Calcite	120	60 (0.25–120)	Portlandite Calcite	Portlandite Calcite	Portlandite Calcite $\text{CaSO}_3 \cdot 1/2\text{H}_2\text{O}$	Portlandite Calcite $\text{CaSO}_3 \cdot 1/2\text{H}_2\text{O}$
<i>Bianco San Giovanni</i> 11416	BSG-C	Portlandite Calcite	Portlandite Calcite	120–1000	120 (0.3–250)	Portlandite Calcite	Portlandite Calcite	Portlandite Calcite $\text{CaSO}_3 \cdot 1/2\text{H}_2\text{O}$	Portlandite Calcite $\text{CaSO}_3 \cdot 1/2\text{H}_2\text{O}$
Gypsum Alabaster, Italian plaster 58340	G-EF	Gypsum	Bassanite Anhydrite	<75	7 (0.2–85)	Bassanite Anhydrite	Gypsum	Bassanite Anhydrite Gypsum $\text{K}_2\text{SO}_4$	Gypsum Bassanite Anhydrite $\text{CaSO}_3$
Natural gypsum 58300 Selenite (Terra Alba)	G-F	Gypsum	Bassanite Anhydrite	80% < 20 18% < 25 1.9% < 32 1.9% < 32	9 (0.2–75)	Anhydrite Gypsum	Anhydrite Gypsum	Anhydrite Gypsum $\text{CaSO}_3$ $\text{K}_{0.67}\text{Na}_{1.33}\text{SO}_4$ $\text{MgS}_2\text{O}_3 \cdot 6\text{H}_2\text{O}$	Anhydrite Gypsum $\text{CaSO}_3$ $\text{K}_{0.67}\text{Na}_{1.33}\text{SO}_4$ $\text{MgS}_2\text{O}_3 \cdot 6\text{H}_2\text{O}$
Gypsum alabaster 58343	G-M	Bassanite	Bassanite Anhydrite	85% < 40	16 (1–160)	Bassanite Anhydrite	Bassanite Anhydrite	Gypsum $\text{CaSO}_3$	Gypsum $\text{CaSO}_3$
Lead white 46000	LW	Basic lead carbonate	Hydrocerussite Cerussite	<45	3 (0.1–10)	Hydrocerussite Cerussite	Hydrocerussite Cerussite	Hydrocerussite Cerussite $\text{Pb}_4\text{O}_3\text{SO}_4 \cdot \text{H}_2\text{O}$ $\text{Pb}_2\text{O}(\text{SO}_4)$ $\text{Pb}_4\text{SO}_4(\text{CO}_3) \cdot 2(\text{OH})_2$	Hydrocerussite Cerussite $\text{Pb}_4\text{O}_3\text{SO}_4 \cdot \text{H}_2\text{O}$ $\text{Pb}_2\text{O}(\text{SO}_4)$ $\text{Pb}_4\text{SO}_4(\text{CO}_3) \cdot 2(\text{OH})_2$

\*: Main maximum particle size and particle size range in parentheses. EF: extra fine size; ST: standard size; C: coarse size; F: fine size; M: medium size; Calcite:  $\text{CaCO}_3$ ; Portlandite:  $\text{Ca}(\text{OH})_2$ ; Gypsum:  $\text{CaSO}_4 \cdot 2\text{H}_2\text{O}$ ; Bassanite:  $\text{CaSO}_4 \cdot 1/2\text{H}_2\text{O}$ ; Anhydrite:  $\text{CaSO}_4$ ; Basic lead carbonate:  $\text{Pb}(\text{CO}_3)_2 \cdot \text{Pb}(\text{OH})_2$ ; Hydrocerussite:  $2\text{PbCO}_3 \cdot \text{Pb}(\text{OH})_2$ ; Cerussite:  $\text{PbCO}_3$ ; Dolomite:  $\text{CaMg}(\text{CO}_3)_2$ ; Quartz:  $\text{SiO}_2$ .

## 2.2. SO<sub>2</sub> Exposure Aging Test

An accelerated alteration test was chosen, exposing the samples to the action of SO<sub>2</sub> gas at a concentration much higher than that normally found in European cities. This was performed because the overall objective of the research, in which this study is integrated, is to compare the susceptibility of tempera paintings made with different pigments to SO<sub>2</sub> gas. For the aging test under SO<sub>2</sub> exposure, a FITOCLIMA 300EDTU (ARALAB, Madrid, Spain) climatic chamber was used in which an atmosphere rich in SO<sub>2</sub> was produced under constant temperature and relative humidity (25 °C and 45% RH). The SO<sub>2</sub> gas was diluted in nitrogen gas at 3%, generating an atmosphere with an SO<sub>2</sub> concentration of 200 ppm, a concentration that exceeds by 5 orders of magnitude the concentration of SO<sub>2</sub> in the atmosphere of most European cities (average value 0.00076 ppm). The SO<sub>2</sub> exposure aging test lasted a total of 2 months. The water used to generate RH was previously analyzed by high resolution liquid chromatography and ICP-OES to determine its composition (anions and cations); the ion composition, which can be consulted in previous works [17,18], was the following: 15.8 mg/L Cl<sup>-</sup>, <0.05 mg/L NO<sub>2</sub><sup>-</sup>, 2.15 mg/L NO<sub>3</sub><sup>-</sup>, 23.7 mg/L SO<sub>4</sub><sup>2-</sup>, 0.017 mg/L Ba<sup>2+</sup>, 17.35 mg/L Ca<sup>2+</sup>, 2.37 mg/L K<sup>+</sup>, 3.74 mg/L Mg<sup>2+</sup> and 13.18 mg/L Na<sup>+</sup>.

## 2.3. Analytical Techniques

The mineralogical composition of the pigments was determined by X-ray diffraction (XDR) using a Siemens (Munich, Germany) D5000 (Cu K $\alpha$  radiation at a voltage of 45 kV and 40 mA intensity and with the incorporation of a Ni filter). A scan was performed between 3 and 60°2 $\theta$  at a goniophotometer speed of 0.05°2 $\theta$  s<sup>-1</sup>. The pigments were analyzed by the random powder method and the identification of mineral phases was made using the X'Pert HighScore software-version 2.2.3 (2007) (Malvern Panalytical Ltd., Worcestershire, UK).

A granulometric analysis (particle grain size) of the pigments was performed by means of laser diffraction (Mastersizer 2000LF, Malvern Panalytical Ltd., Worcestershire, UK). For this, the samples were dispersed in alcohol, and the results were expressed on volume distribution.

Regarding the paintings, the same analytical approach used in [18,19] was applied to characterize them before and after the SO<sub>2</sub> exposure aging test:

The appearance of the mock-up surfaces (references and aged samples) was studied by means of stereomicroscopy (SMZ 1000, Nikon, Tokyo, Japan); the observation and imaging conditions (light intensity, light temperature and RGB sensor balance) were the same for all observations, so all images are completely comparable.

The color of the surface of references and aged samples was characterized in the CIELAB and CIELCH spaces [21] using a Minolta CM-700d spectrophotometer (Konica Minolta Inc., Tokyo, Japan). The parameters collected were the color coordinates  $L^*$ ,  $a^*$  and  $b^*$ :  $L^*$  corresponds to the color lightness and ranges from 0 (black) to 100 (white);  $a^*$  indicates the position between red (positive values) and green (negative values), and  $b^*$  between yellow (positive values) and blue (negative values). For each surface, nine measurements were collected using D65 as an illuminant, in Specular Component Included (SCI) mode, with a 3 mm spot diameter and with an observer angle of 10°. To evaluate the color changes produced after the aging test, the colorimetric differences ( $\Delta L^*$ ,  $\Delta a^*$  and  $\Delta b^*$ ) and color difference ( $\Delta E^*_{ab}$ ) were calculated, using the color data of not-exposed mock-ups as reference.

The gloss variation ( $\Delta G$ ) between the references and the aged paints was obtained with a glossmeter Konica Minolta Unigloss 60Plus (Konica Minolta Inc., Tokyo, Japan). Three measurements per surface were recorded at a reflection angle of 60°.

Changes on the reflectance of the paints were also studied with a hyperspectral camera equipped with a CCD sensor Pulnix (Sunnyvale, CA, USA) TM-1327 GE (1040 rows, 1392 columns), an optical system with objective lenses (10 mm focal length) and a Specim (Oulu, Finland) ImSpector V10 spectrograph (spectral resolution of 4.55 nm) located between the lenses and the sensor. The spectral camera captured a linear array of 1392 pixels across 1040 wavelengths spanning the range of 400–1000 nm. The spectral range selected for the spectra was 450–700 nm. The camera scanned the surface line by line as the target sample was moved vertically, capturing an image at each of the 1040 wavelengths. As a light source, a Schott DCR<sup>®</sup> III incandescent lamp (SCHOTT AG, Mainz, Germany) with a rectangular head (51 mm long and 0.89 mm wide) was used. A cylindrical lens positioned in front of the lamp focused the light into an illuminated area measuring 15 cm in length and 1 cm wide. To scan the entire surface of each mock-up, a motorized XYZ translation stage was used to move the sample. The data from the hyperspectral images were processed using the MATLAB-R2022b (The MathWorks, Inc. Madrid, Spain) program to obtain the corresponding reflectance graphs.

To characterize the textural modifications on the surface of the aged paint mock-ups comparatively to reference samples, changes in roughness were evaluated using a profilometer (Mitutoyo SJ400, Mitutoyo America Corporation, Aurora, IL, USA) and analyzing the variations in the average maximum profile height ( $R_z$ ,  $\mu\text{m}$ ) [22]. Then, 3 profiles per sample were obtained, scanning a minimum length of 2 cm.

The hydrophobic nature of the surface of the paints before and after the aging test was studied by determining the static contact angle ( $^\circ$ ) by means of an SEO Phoenix-300 Touch goniometer (SEO, Saneopro, Gyeonggi-do, Republic of Korea), applying the sessile drop method and using for this a droplet of 6  $\mu\text{L}$  of deionized water [23]. Then, 3 measurements per analyzed surface were obtained at laboratory conditions ( $18 \pm 5$   $^\circ\text{C}$ ;  $60 \pm 10\%$  RH).

Mineralogic analyses of the tempera paints (references and aged samples) were performed by XRD using the equipment and measurement conditions explained above, and chemical and molecular analyses were also performed by means of a diamond crystal Attenuated total reflection (ATR)-Fourier transform infrared spectroscopy (FTIR); for this, a Thermo Nicolet 6700 (Thermo Fisher Scientific, Waltham, MA, USA) was used, and it recorded 32 scans per sample from 4000 to 400  $\text{cm}^{-1}$  with a 2  $\text{cm}^{-1}$  resolution.

Chemical and micro-morphology changes produced after the aging test were studied under Scanning Electron Microscopy (SEM) with energy-dispersive X-ray spectroscopy (EDS), analyzing carbon-sputtered surfaces of the reference and aged paint mock-ups. For this, a piece of Philips (Koninklijke Philips N.V., Amsterdam, The Netherlands) XL30 (equipment (9–11 mm of working distance, 60 mA of specimen current) was used, using Secondary Electron (SE) and Back Scattered Electron (BSE) detection modes; X-ray spectra were obtained by applying a 20 kV of accelerating voltage a recording during 40–60 s of dwell acquisition time.

### 3. Results

#### 3.1. Pigment Characterization

XRD confirmed that the mineralogical composition of the white pigments differed to that reported by the manufacturer (Table 1); a similar finding was obtained in [24]. The exception was for Bianco di San Giovanni pigments (BSG-ST and BSG-C) which were composed by portlandite ( $\text{Ca}(\text{OH})_2$ ) and calcite ( $\text{CaCO}_3$ ) as informed by the manufacturer. CA-EF pigment was composed of calcite, though dolomite ( $\text{CaMg}(\text{CO}_3)_2$ ) was identified as an impurity; a similar finding was reported in [6]. In gypsum pigments G-EF and G-F, rather than gypsum (as reported by the manufacturer), bassanite ( $\text{CaSO}_4 \cdot 1/2\text{H}_2\text{O}$ ) and anhydrite ( $\text{CaSO}_4$ ) were identified (Table 1). Bassanite was present in GM (according

to the manufacturer), however anhydrite was also identified. LW pigment, which is sold as basic lead carbonate ( $\text{Pb}(\text{CO}_3)_2 \cdot \text{Pb}(\text{OH})_2$ ), is actually composed of hydrocerussite ( $2\text{PbCO}_3 \cdot \text{Pb}(\text{OH})_2$ ) and cerussite ( $\text{PbCO}_3$ ), as reported in the literature [25].

Regarding the pigments' grain size, some inaccuracies were found between values reported by the manufacturer and the experimental data (Table 1), as found elsewhere [13,18,19]. For example, for pigment CA-EF, a grain size of 20  $\mu\text{m}$  was reported by the manufacturer, while the laser diffraction detected a maximum particle size of 25  $\mu\text{m}$  and a range from 0.25 to 100  $\mu\text{m}$ . Moreover, it is noticeable that for pigment BSG-C, we detected a grain size range between 0.3 and 250  $\mu\text{m}$  whereas the manufacturer stated a range between 120 and 1000  $\mu\text{m}$ . In the case of gypsum pigments, differences with the sizes reported by the manufacturer were also detected. For the G-EF pigment, a grain size lower than 75  $\mu\text{m}$  was reported, while a maximum grain size of 7  $\mu\text{m}$  and a range from 0.2 to 85  $\mu\text{m}$  were experimentally obtained. For the G-F pigment, the grain size stated by the manufacturer was lower than 32  $\mu\text{m}$  while the size range here found was from 0.2 to 75  $\mu\text{m}$ , with a main maximum particle at 9  $\mu\text{m}$ . For the G-M pigment, a grain size lower than 40  $\mu\text{m}$  was reported by Kremer while the real maximum grain size was 16  $\mu\text{m}$ , with the range between 1 and 160  $\mu\text{m}$ . Likewise, for pigment LW, the manufacturer indicated a grain size lower than 45  $\mu\text{m}$ , although the primary particle size was 3  $\mu\text{m}$  with a size range from 0.1 to 10  $\mu\text{m}$ .

### 3.2. Physical, Mineralogical and Chemical Changes of the Mock-Ups After $\text{SO}_2$ Exposure Aging Test

Stereomicroscopy observations made on the paintings before being tested revealed an influence of the grain size on the roughness of the paints, since paints made with coarser pigments had rougher surfaces (Figure 1). For example, the surfaces of BSG-C-based paints showed greater irregularity since the pigment used was the coarsest. The paint surfaces showed surfaces with circular pockmarks, assigned to relics of air bubbles. Moreover, in LW-E paint, where the pigment had the smallest grain size (3  $\mu\text{m}$ ), it was possible to see the brush strokes (Figure 1). On the other hand, some paint mock-ups containing egg yolk often showed a higher yellow coloring (due to the binder tint) than their counterparts made with rabbit glue. (See Figure 1, CA-EF-E, BSG-ST-E, BSG-C-E, G-EF-E, G-F-E).

The  $\text{SO}_2$  aged paints did not show any visible modification of their surfaces in comparison with the reference paints (Figure 1). However, the spectrophotometry results (Figure 2) revealed that some paints (i.e., CA-EF-E, BSG-ST-E and G-F-R) suffered  $\Delta E^*_{ab}$  higher than 3.5 CIELAB units, which is the threshold above which a color change is visible by a non-expert observer [26]. Therefore, considering  $\Delta E^*_{ab}$ , the aged paint CA-EF-E showed the highest color change, while the aged paint G-M-R showed the lowest color change. The most affected colorimetric parameter after the  $\text{SO}_2$  test was  $b^*$  for most of the samples, except for the rabbit-glue-based paints, G-EF-R and WL-R, and the egg-yolk-based paint with BSG-C. The  $b^*$  parameter in the egg yolk paints typically exhibited a decrease (except for paints BSG-C-E and WL-E) suggesting the loss of the characteristic yellow coloration of the egg yolk paints, as was stated in [13]. Conversely, in the rabbit glue paints,  $b^*$  suffered an increase (except G-M-R) resulting in a yellowing effect. In BSG-C-E, G-EF-R and WL-R, the most affected parameter was  $L^*$ , showing a decreasing trend.

The  $L^*$  parameter increased in the egg-yolk-based paints, with the exception of the BSG paints, demonstrating a whitening effect on their color. Conversely,  $L^*$  diminished in all rabbit-glue-based paints, except for CA-EF-R. The color difference  $\Delta E^*_{ab}$  was higher in the egg-yolk-based paints comparatively to those made with rabbit glue, with the exception of paints made with G-F. Therefore, egg-yolk-based paints experienced the most intense colorimetric change in comparison to the rabbit-glue-based paints.

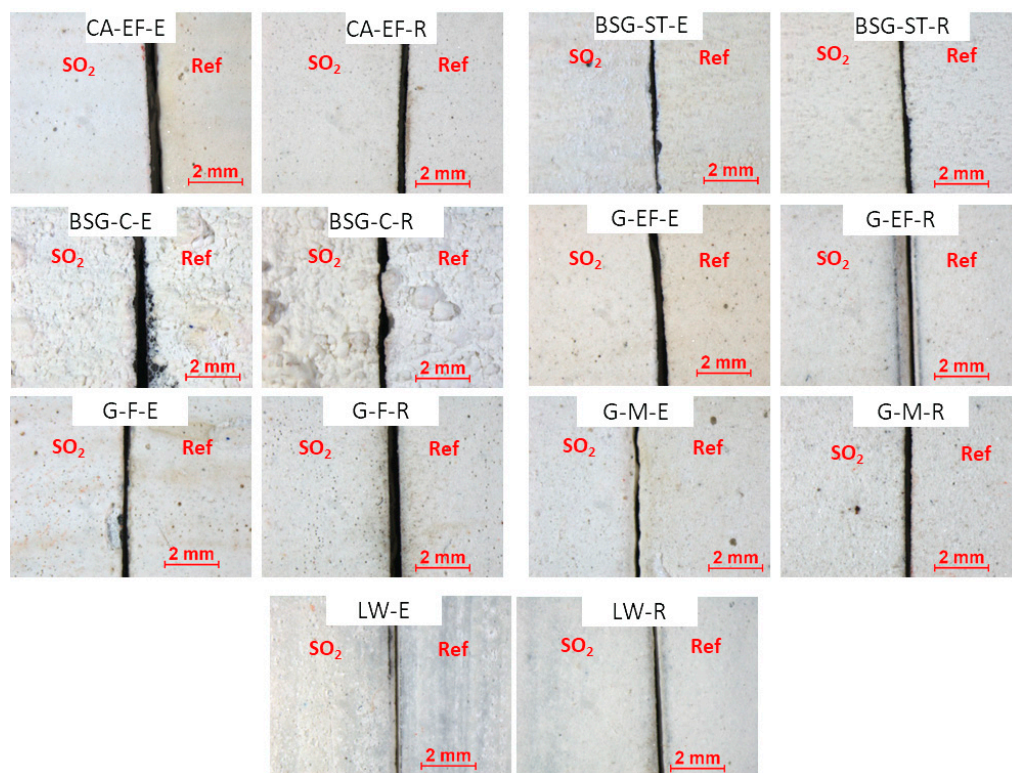


**Figure 1.** Photomicrographs taken with stereomicroscopy of the references (Ref, on the (right)) and the aged paint mock-ups (SO<sub>2</sub>, on the (left)). Check Table 1 for the identification code of samples.

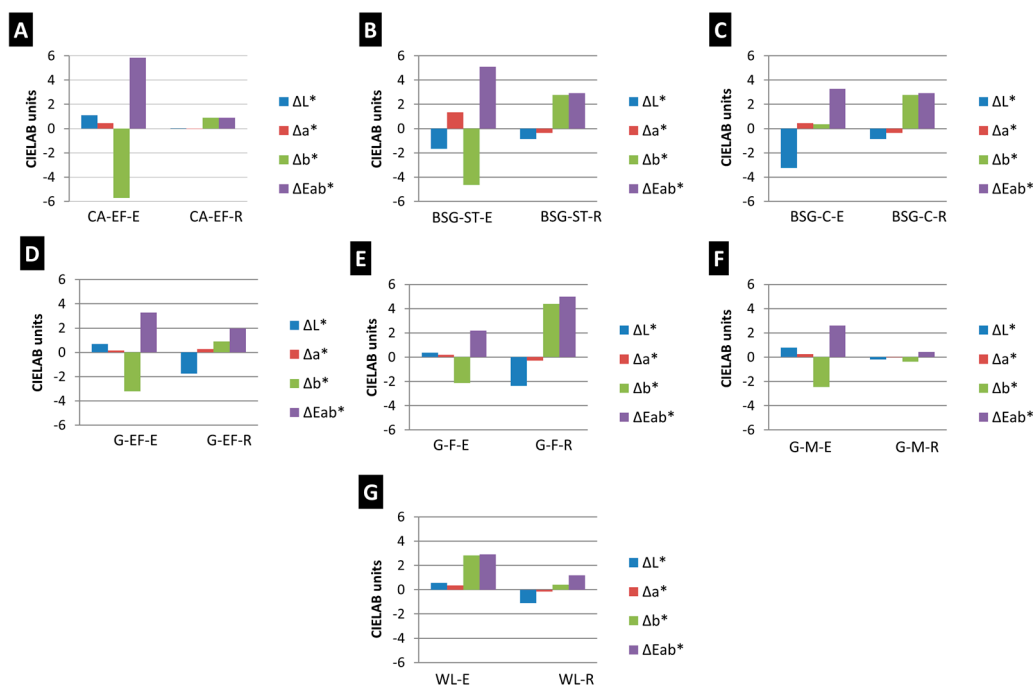


**Figure 2.** Differences on colorimetric parameters  $\Delta L^*$ ,  $\Delta a^*$  and  $\Delta b^*$  and color difference  $\Delta E^*_{ab}$  suffered by the aged paints considering the original color of the paints before aging as reference. (A–C) calcite-, (D–F) gypsum- and (G) lead white-based paints. Check Table 1 for the identification code of samples.

Gloss variations ( $\Delta G$ ) after the SO<sub>2</sub> exposure test were not important except for two samples: the egg-yolk-BSG ST paint and the rabbit-glue-G EF paint. It was not possible to find out a relation between the gloss variation and the type of binder (Figure 3). The data

for this property showed no relationship between the magnitude of the change and the type of binder or pigment grain size.

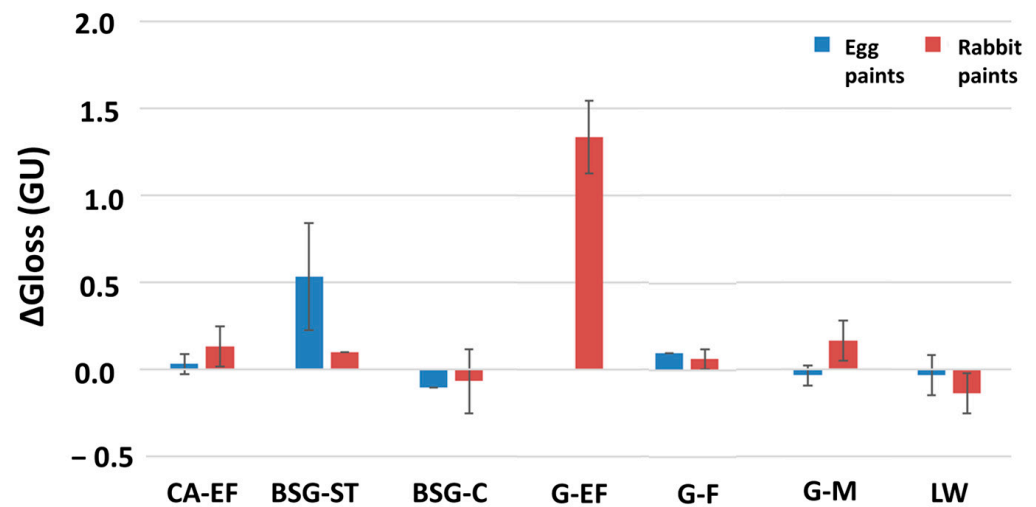
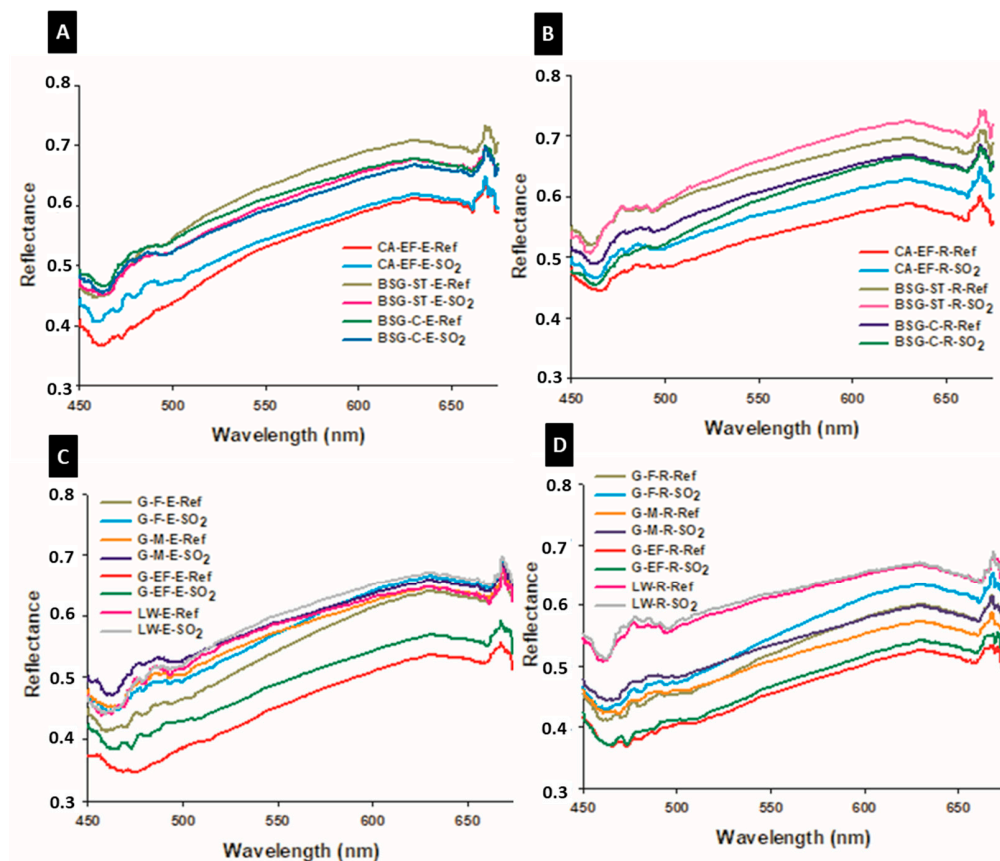


**Figure 3.** Gloss variations ( $\Delta G$ ) of the aged paint mock-ups. Check Table 1 for the identification code of samples.

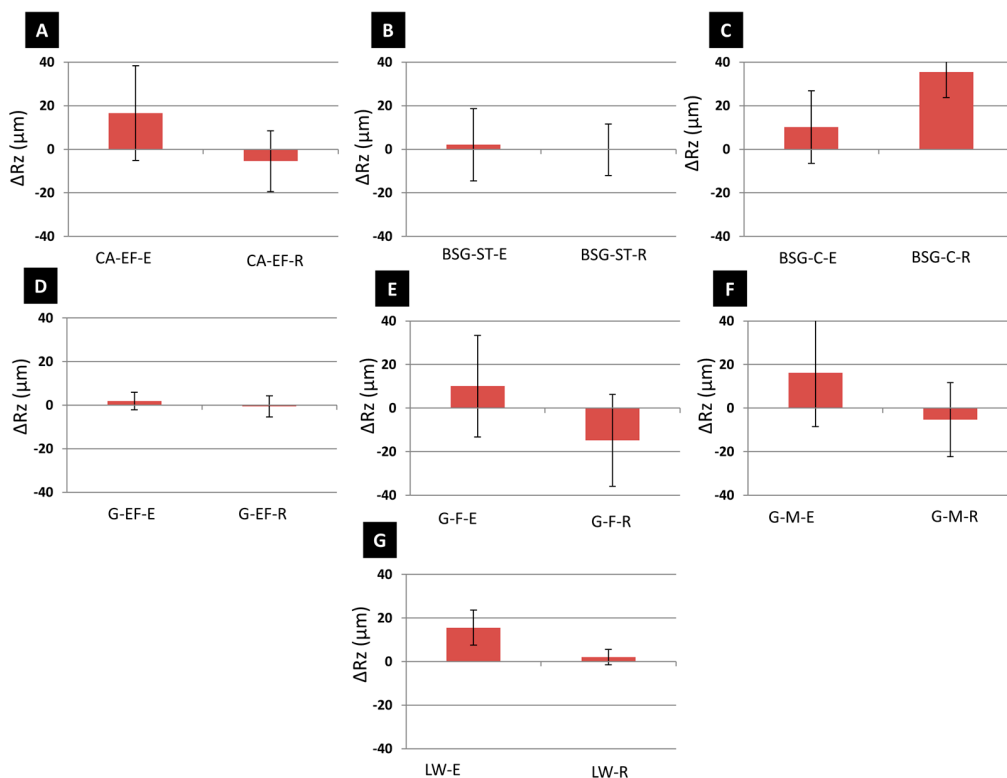
The reflectance spectra of the reference and the aged paint mock-ups are depicted in Figure 4. In agreement with [27], we found that, before the aging test, the morphology of the spectral curve of the reference mock-ups prepared with the same pigment was similar regardless of the binder used. However, differences were found in the reflectance intensity between the samples made with the same pigment though with a different binder. Thus, the reference paints made with rabbit glue (Figure 4B,D) showed in the lower region of the spectrum (450–500 nm) higher reflectance values than those prepared with egg yolk (Figure 4A,C), except for the paints made with G-M and G-F (Figure 4C,D). However, and contrary to what has been found in previous studies [28], the reflectance intensity did not show a relation with the grain size of the pigment. After the SO<sub>2</sub> aging test, the intensity of the reflectance increased in all the mock-ups, except in the paints prepared with pigments BSG-ST and BSG-C mixed with egg yolk (Figure 4A).

Figure 5 shows the roughness variation after the aging test. In general, egg-yolk-based paints suffered roughness increases and rabbit-glue-based paints experienced roughness decreases, except for the BSG-C-R paint mock-up (Figure 5C) and, to a lesser extent, the LW-R paint mock-up (Figure 5G). Moreover, although there were not statistical differences between the paints made with egg yolk or rabbit glue, those prepared with egg yolk showed higher R<sub>z</sub> variations than those made with rabbit glue, except for the BSG-C and G-F paints.

The mineralogical analyses carried out on the paints before being subjected to the test yielded interesting results when comparing the X-ray diffractograms of the paints with those of the original pigments before mixing them with the binders (Table 1). Thus, new mineral phases were identified, which suggest an interaction between the pigment and the binder during the drying process of the paint, as reported in previous studies for other pigments [19]. In paints made with G-F, gypsum and anhydrite were detected, though the pigment contained bassanite and anhydrite. This occurred in both egg-yolk- and rabbit-glue-based paints. Something similar happened to the GE-F-R paint since the original pigment was made of bassanite and anhydrite, though only gypsum was detected in the paint.



**Figure 4.** Reflectance spectra of reference (-Ref) and aged (-SO<sub>2</sub>) paint mock-ups. Check Table 1 for the identification codes of samples. (A,C): egg-yolk-based paints. (B,D): rabbit-glue-based paints.



**Figure 5.** Variation of the average maximum profile height ( $\Delta R_z$ ,  $\mu\text{m}$ ) of the tempera paint mock-ups after SO<sub>2</sub> aging. (A–C) calcite-, (D–F) gypsum- and (G) lead white-based paints. Check Table 1 for the identification codes of samples.

After the SO<sub>2</sub> aging test, the formation of new mineral phases in all the paint mock-ups was detected by means of XRD (Table 1). In CA-EF paints, calcium sulfite (Ca<sub>3</sub>(SO<sub>3</sub>)<sub>2</sub>SO<sub>4</sub>·2H<sub>2</sub>O) was formed in the egg yolk mock-up whereas gypsum was formed in the rabbit glue mock-up. In BSG-ST and BSG-C mock-ups (both in egg-yolk- and rabbit-glue-based paints), calcium sulfite hemihydrate (CaSO<sub>3</sub>·1/2H<sub>2</sub>O) formed.

In G-based aged paints, in addition to the diverse calcium sulfates detected in the corresponding reference paints (i.e., bassanite, gypsum and/or anhydrite), different neo-formed calcium-sulfate minerals were identified. Accordingly, in G-EF-E aged paint, bassanite, anhydrite, gypsum and K<sub>2</sub>SO<sub>4</sub> were detected (Table 1), while bassanite, anhydrite, gypsum and CaSO<sub>3</sub> were found in G-EF-R aged paint. Neo-formed minerals were more varied in the G-F-based aged paints where calcium (Ca), potassium (K), sodium (Na) and magnesium (Mg) sulfates and sulfites were identified (Table 1). Conversely, gypsum and CaSO<sub>3</sub> were the only minerals detected in the G-M aged paints. Finally, in the LW-based aged paints, in addition to hydrocerussite and cerussite, neo-formed Pb-based sulfates and carbonates were found, i.e., Pb<sub>4</sub>O<sub>3</sub>SO<sub>4</sub>·H<sub>2</sub>O, Pb<sub>2</sub>O(SO<sub>4</sub>) and Pb<sub>4</sub>SO<sub>4</sub>(CO<sub>3</sub>)<sub>2</sub>(OH)<sub>2</sub>.

FTIR analyses allowed the identification of absorption bands assigned to the binders, the inorganic pigments and the neo-formed minerals identified in the aged paint mock-ups (Figure 6). On the one hand, the FTIR spectra of the egg yolk binder showed a broad band at 3266 cm<sup>-1</sup> assigned to O–H stretching or/and N–H stretching from proteins, together with bands at 2921 cm<sup>-1</sup> assigned to C–H asymmetric stretching, and at 2850 cm<sup>-1</sup> assigned to C–H symmetric stretching from long chain fatty acids. Also, bands between 1785 and 1720 cm<sup>-1</sup> assigned to C=O asymmetric stretching were detected, as well as a band at 1620 cm<sup>-1</sup> due to C=O stretching from amide I, in addition to a band at 1530 cm<sup>-1</sup> assigned to N–H bending from amide II. Bands at 1440 and 1365 cm<sup>-1</sup> were also observed, assigned to bending vibrations of CH<sub>2</sub> groups and CH<sub>3</sub> groups of amino acid side chains, respectively. Likewise, a band at 1230 cm<sup>-1</sup> due to C–N stretching and N–H bending vibrations of amide III, bands between 1160 and 1041 cm<sup>-1</sup> (stretching vibration of the C–O group of glycerol) and 956 cm<sup>-1</sup> (twisting vibration of CH<sub>2</sub> group of glycerol) [14,29,30] were found.

On the other hand, the FTIR spectra of the rabbit glue binder showed bands at 3290 cm<sup>-1</sup> assigned to O–H symmetric stretching or/and N–H stretching from proteins, at 2871 cm<sup>-1</sup> assigned to C–H symmetric stretching, and at 1620 cm<sup>-1</sup> associated with C=O stretching from amide I. A band at 1520 cm<sup>-1</sup> assigned to C–N stretching and N–H bending from amide II was also found. Finally, bands between 1400 and 1000 cm<sup>-1</sup> were associated with collagen absorption features attributed to CH<sub>2</sub> wagging, CH<sub>3</sub> deformation, C–N stretching and C–O stretching [13,31].

Regarding the reference paints, in the CA- and BSG-based paints, calcite was identified through their characteristic C–O bands: the most intense at 1409 cm<sup>-1</sup>, and weaker ones at 874 and 725 cm<sup>-1</sup> assigned to CO<sub>3</sub><sup>2-</sup> stretching [32]. Compared to calcite, dolomite displayed characteristic FTIR absorption bands at 3020, 2626 and 730 cm<sup>-1</sup> [33]. Surprisingly, although dolomite was identified in the reference CA-EF-E paint by using XRD, the FTIR analysis did not allow the detection of the aforementioned bands assigned to this mineral. Portlandite was identified by XRD in several reference and aged mock-ups (Table 1). In the FTIR spectra, the presence of this mineral was confirmed through a strong band around 3680 cm<sup>-1</sup>, which was assigned to O–H stretching vibration of portlandite [34].



For the reference G-based paints, the sulfate ion (S–O) of gypsum was detected through four fundamental vibration modes: bands  $\sim 980\text{ cm}^{-1}$  due to  $\text{SO}_4^{2-}$   $v_1$  symmetric stretching vibration,  $\sim 450\text{ cm}^{-1}$  due to  $\text{SO}_4^{2-}$   $v_2$  symmetric bending vibration,  $\sim 1100\text{ cm}^{-1}$  for  $\text{SO}_4^{2-}$   $v_3$  symmetric bending and  $\sim 610\text{ cm}^{-1}$  for the  $\text{SO}_4^{2-}$   $v_4$  asymmetric bending vibration [35,36]. Considering the diverse calcium sulfate minerals (gypsum, bassanite and anhydrite), small shifts can be found among the FTIR spectra bands [36]. The  $\text{SO}_4^{2-}$   $v_1$  vibration was found at 1017, 1015 and  $1008\text{ cm}^{-1}$  for anhydrite, bassanite and gypsum, respectively, being more intense in bassanite and almost inappreciable in anhydrite [36,37]. Gypsum, bassanite, and anhydrite all exhibited a doublet for the  $v_2$  symmetric bending of the  $\text{SO}_4^{2-}$  tetrahedra at 439 and  $415\text{ cm}^{-1}$ , 489 and  $427\text{ cm}^{-1}$  and 499 and  $416\text{ cm}^{-1}$ , respectively. The  $\text{SO}_4^{2-}$   $v_3$  symmetric bending was identified through two bands at 667 and  $595\text{ cm}^{-1}$  for gypsum, at 659 and  $594\text{ cm}^{-1}$  for bassanite and three bands at 672, 610 and  $591\text{ cm}^{-1}$  for anhydrite [37]. For the  $v_3$  antisymmetric stretching vibration, the strongest absorption peaks were found at 1111, 1102 and  $1094\text{ cm}^{-1}$  for bassanite, gypsum and anhydrite, respectively [37]. For the  $v_4$  antisymmetric bending vibration modes, the identified bands were those at 676, 629 and  $612\text{ cm}^{-1}$  in anhydrite, 668 and  $628\text{ cm}^{-1}$  in bassanite and 670 and  $620\text{ cm}^{-1}$  in gypsum [37]. Additionally, we found (i) for gypsum, O–H stretching vibrations at 3500 and  $3394\text{ cm}^{-1}$  and O–H bending vibration at 1680 and  $1619\text{ cm}^{-1}$ , and (ii) for bassanite, O–H stretching vibrations around 3600 and  $3540\text{ cm}^{-1}$  and O–H  $v_1$  bending vibration at  $1617\text{ cm}^{-1}$  [37].

For the reference LW-based paints, the presence of hydrocerussite was detected due to the presence of O–H stretching vibrations assigned to the band at  $3530\text{ cm}^{-1}$ , C–O vibration modes of  $\text{CO}_3^{2-}$  anions at  $1733\text{ cm}^{-1}$  corresponding to the  $v_1 + v_4$  combination mode of  $\text{CO}_3^{2-}$  anions,  $1384\text{ cm}^{-1}$  ( $v_3$  asymmetric C–O stretching vibrations),  $1041\text{ cm}^{-1}$  ( $v_1$  symmetric C–O stretching vibrations),  $837\text{ cm}^{-1}$  ( $v_2$  out-of-plane bending vibrations) and  $676\text{ cm}^{-1}$  ( $v_4$  in-plane bending vibrations) [38]. The shoulder at  $1052\text{ cm}^{-1}$  and the bands at 1041 and  $960\text{ cm}^{-1}$  can be assigned to  $\text{SO}_4^{2-}$  anions [38]. Regarding the bands assigned to the cerussite, they could be overlapped by hydrocerussite [38].

After the  $\text{SO}_2$  test, increases on the absorbance of the S–O FTIR characteristic bands were observed in the spectra of samples BSG-ST, BSG-C, G-M, G-F, G-EF and, to a lesser extent, in the WL spectra. In all these cases, these modifications were found both in the paints made with egg yolk and in those made with rabbit glue. These S–O FTIR bands were attributed to the different species of sulfites and sulfates that formed in the samples after the test. In BSG-ST, BSG-C, G-M and G-EF paints, new FTIR bands appeared around  $640\text{ cm}^{-1}$  ( $v_4$  asymmetric bending vibration of S–O group),  $980\text{ cm}^{-1}$  ( $v_1$  symmetric stretching vibration of S–O) and  $1100\text{ cm}^{-1}$  ( $v_3$  symmetric bending vibration). In the paints made with LW, the identification of only one new peak at  $640\text{ cm}^{-1}$  was noticeable, considering that two species of lead sulfate were found by XRD.

By SEM-EDS, the formation of deposits of a different nature was observed after the  $\text{SO}_2$  exposure test (Figure 7). On CA-based paints (Figure 7A,B), scarce calcium-rich deposits, and to a lesser extent, deposits rich in Na, Mg, silica (Si), sulfur (S) and chlorine (Cl) (pointed out with an arrow in Figure 7B), were found on the aged surfaces of egg-yolk- and rabbit-glue-based paints. On the BSG-based paints, micrometric particles, already found in the reference paints (pointed out with a rectangle in Figure 7C,E), were also detected in the aged ones (pointed out with a rectangle in Figure 7D,F). Moreover, deposits rich in S and Ca on the surfaces (with an atomic ratio of S:Ca, similar to that of gypsum) were also identified on the BSG aged samples. As for the BSG-C aged paints made with egg yolk we observed that grain minerals were more intensely agglomerated when compared to the reference paints (Figure 7F and Figure 7E, respectively).

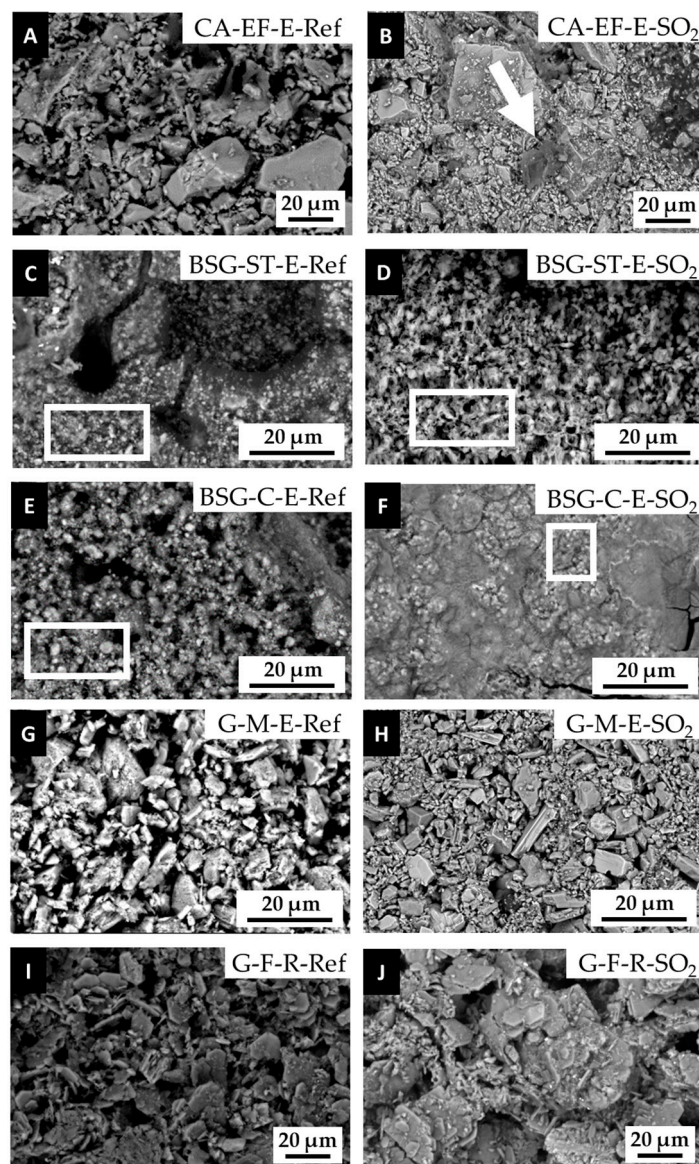


**Figure 7.** SEM micrographs of CA-, BSG- and G-based paint mock-ups made with egg yolk or rabbit glue. -Ref = reference paints; -SO<sub>2</sub> = aged paints. (A–F) calcite- and (G–J) gypsum- based paints. Check Table 1 for the identification codes of the samples. Arrow pointed out deposits rich in Ca and at lesser extent Na, Mg, Si, S and Cl. Rectangles show micrometric particles.

No remarkable differences were detected after exposure to SO<sub>2</sub> on the G-based paints (Figure 7G–J). Regarding the aged LW paint mock-ups, SEM observations did not allow the identification of neo-formed minerals, although different phases of lead sulfates were already identified by XRD. Nonetheless, EDS analyses confirmed an enrichment of S on the surface of the paints. Moreover, no major differences in texture or in the amount and type of surface deposits were detected in the LW paints made of either rabbit glue or egg yolk.

#### 4. Discussion

Attending to the colorimetric changes, paints made with egg yolk showed higher  $\Delta E^*_{ab}$  in comparison to their rabbit glue counterparts, suffering a loss of their original yellowish coloration and a whitening of the surface. It is suggested that this whitening effect could be related to the physical degradation of the binder (which gave to unaltered paints a subtle yellowish color) and to the formation of white sulfate and sulfite salts (identified by XRD, FTIR and SEM) due to the SO<sub>2</sub> aging test. In previous articles focused on the study of the

deterioration of blue and green paint mock-ups (rabbit-glue- or egg-yolk-based paints with lapis lazuli, smalt, azurite or malachite) under the same aging test conditions [18,19], it was detected that paints made with egg yolk exhibited higher colorimetric changes (i.e., whitening) than those made with rabbit glue. In the referred works, this colorimetric change was also attributed to the sulfate salts deposited on the paint surfaces, which were more abundant in egg yolk paints. In the current research, XRD revealed the formation of diverse phases of sulfites and sulfates after the aging test, which confirms the sulfation of the paint surfaces due to their interaction with  $\text{SO}_2$ . Through this interaction process, the dissolution of the pigments contained in the paint samples, i.e., calcium carbonate in the CA and BSG-based paints, calcium sulfate in the G-based paints and lead carbonate in the WL-based paints, could take place, leading to the subsequent precipitation of sulfites and sulfates, whether calcium (preferably in paints made with calcium carbonate and gypsum) or lead (in the case of WL-based paints).

After the  $\text{SO}_2$  exposure of BSG-based paints, calcium sulfite hemihydrate was formed, which could subsequently transform into gypsum [6]. In these paints, portlandite was still detected in the aged samples regardless of the binder, revealing that the carbonation was not complete after 2 months of exposure. In the case of the egg-yolk-based paints, several authors [6] assigned the presence of portlandite to the existence of a long-lasting superficial film of binder surrounding the portlandite particles, impeding the diffusion of  $\text{CO}_2$  and consequently lowering the carbonation rates.

In the reference CA-EF-R paint, calcite and portlandite were found, however the latter was lacking in the corresponding aged paint, where gypsum was identified. As was reported elsewhere [6], portlandite is much more hygroscopic and soluble than calcite and, thus, in the absence of egg yolk binder (which according to [6] protects the portlandite grains against carbonation) can also react with  $\text{SO}_2$  to form calcium sulfite/sulfate. This reaction only occurs in the presence of water or sufficiently high relative humidity levels [39]. Cultrone et al. [40] have already recognized the important role of portlandite in the fixation of  $\text{SO}_2$  as sulfates. According to these authors, the high pH created by the dissolution of portlandite facilitates  $\text{SO}_2$  absorption and hydrolysis, leading to the formation of sulfite and subsequent oxidation of sulfate ions which react with  $\text{Ca}^{2+}$  and, ultimately, precipitate as gypsum.

On  $\text{SO}_2$  aged LW mock-ups, lead sulfates were identified, which would indicate that the lead carbonate cerussite was partially dissolved, a process that was expected considering the slightly acidic environment involving sulfation by the deposition of  $\text{SO}_2$ .

Moreover, K, Na and Mg sulfates were detected by means of XRD on the G-EF and G-F paints. In addition, Cl was also identified in the calcium-based samples using SEM-EDS. These elements (K, Na, Mg and Cl) could be derived from the water used in the  $\text{SO}_2$  test environment, leading to the precipitation of sulfated or hydrated salts, such as  $\text{K}_2\text{SO}_4$ ,  $\text{K}_{0.67}\text{Na}_{1.33}\text{SO}_4$  and  $\text{MgS}_2\text{O}_3 \cdot 6\text{H}_2\text{O}$  (detected by XRD).

Considering the formation of diverse phases of sulfites and sulfates after the aging test, it is important to highlight that the climatic chamber, in addition to having exposure to  $\text{SO}_2$  gas (diluted at 3% in 3000 ppm of nitrogen and dosed at a concentration of 200 ppm), was also set to 25 °C and 45% RH for two months. The relative humidity value chosen was not too high, but it is important to clarify that RH is a highly influential factor in the chemical-mineralogical alteration process of carbonate materials. Water in the vapor phase can condense on and inside the carbonated paint and, in the presence of  $\text{SO}_2$ , contribute to the dissolution of calcite, causing the release of more  $\text{Ca}^{2+}$  ions that can precipitate as sulfites or sulfates [40]. Therefore, it is very likely that if this research had been conducted with higher RH values (around 90%), more phases of sulfites and sulfates would have

appeared. This topic could be further investigated in the future by subjecting paintings made with these pigments to different levels of temperature and relative humidity.

Concerning the reflectance measurements, the results confirmed changes on the aged paints. Indeed, the increase on the intensity of the reflectance detected in the aged paints could be explained considering the formation of new sulfur-based phases [18,19]. In this study, however, a greater susceptibility of the egg yolk-based paints to the SO<sub>2</sub> deposition process was not confirmed, unlike what was found in previous studies [18,19] where blue (smalt, azurite, lapis lazuli) and green (malachite) tempera paints were subjected to the same SO<sub>2</sub> aging test. Firstly, neither by XRD nor by SEM-EDS, was a greater quantity of S-rich deposits detected on the egg-yolk-based paints, unlike in [19] where a greater quantity of sulfated salts (as product of SO<sub>2</sub> deposition) was found in egg-based paints. Furthermore, the deterioration of the binder was unequivocally confirmed in the previously cited studies [18,19], namely, a higher degree of cracking in rabbit-glue-based paints and an opacification of the egg-yolk-based paints surfaces [18]. The egg yolk binder opacification was explained as a result of the photo-oxidation of their lipids, which, following several studies [6], led to a formation of peroxy radicals and the denaturation of proteins (polymerization of proteins and/or crosslinking of peptide chains). In our study, only differences between egg-yolk- and rabbit-glue-based paints were detected in terms of color and roughness. That is, in egg-yolk-based paints, color suffered a whitening, and roughness varied more intensely (showing increases) than in rabbit-glue-based paints.

Considering that fewer salt deposits were detected in egg-yolk-based paints compared to those made with rabbit glue, these changes in color and roughness were due to a differential degradation of the binders (organic phase) during the aging test. However, no evidence of this deterioration was detected by FTIR or SEM. FTIR only identified changes in the bands assigned to the S–O group (which were associated with the newly formed sulfates and sulfites), and no changes were detected in the functional groups of the binder. On the other hand, SEM did not detect a more intense physical deterioration in egg-yolk-based paints. Probably, the analytical techniques here applied were not the most suitable for detecting minor chemical or physical modifications in the binders. However, it is indisputable from the point of view of roughness and color, that a greater physical deterioration in egg-yolk-based paints took place. This greater deterioration could be explained by differences in the degree of hydrophilicity of the paints. The determination of the static contact angle in our tempera mock-ups allowed us to confirm that paints made with egg yolk were hydrophilic (static contact angle lower than 90°, [41]) while paints made with rabbit glue showed static contact angle values above 90°, thus showing a hydrophobic behaviour (Table 2). This would determine a greater susceptibility to deterioration of the egg yolk binder that could manifest itself in a greater change in roughness and color.

**Table 2.** Static contact angle ( $\theta^\circ$ ) of the reference paint mock-ups. Check Table 1 for the identification codes of the samples.

Authors' Identification Code	Egg-Yolk-Based Samples	Rabbit-Glue-Based Samples
CA-EF	56.82 ± 6.33	120.58 ± 2.68
BSG-ST	83.20 ± 1.83	127.63 ± 3.94
BSG-C	96.97 ± 2.28	114.12 ± 3.73
G-EF	111.93 ± 2.05	114.84 ± 1.34
G-F	86.45 ± 2.13	115.55 ± 6.65
G-M	90.17 ± 4.14	113.39 ± 1.41
WL	93.70 ± 1.87	98.67 ± 1.03

## 5. Conclusions

In this research, white tempera mock-ups composed of a pigment (calcite, Bianco di San Giovanni, gypsum or lead white) mixed with an organic binder (rabbit glue or egg yolk) were exposed to a SO<sub>2</sub>-rich atmosphere in order to evaluate the physical, chemical and mineralogical changes. Firstly, verifying the composition and grain size of pigments was crucial to ensure reliable and accurate results. It was confirmed that these tempera paints were susceptible to sulfation which resulted from SO<sub>2</sub> deposition. This sulfation was revealed through the formation of sulfur-based salts (both sulfates and sulfites) because of the dissolution of the pigments. The amount of salts formed was similar in paints made with egg yolk and rabbit glue, contrary to what was found in tempera paint mock-ups made with other pigments subjected to the same SO<sub>2</sub> aging test. Therefore, it can be concluded that, in the case of tempera paints made with calcite, gypsum and lead carbonate, the nature of the binder (egg yolk or rabbit glue) did not influence the reactivity to sulfation by means of SO<sub>2</sub> gas exposure. Spectrophotometry confirmed that the color of the paints slightly changed after aging, more intensely in egg-yolk-based paints. In these paints, a greater modification of roughness was also detected after the SO<sub>2</sub> test. Given that the amount and type of salts formed was similar in the paints regardless of the binder, the changes in color and roughness in the egg-yolk-based tempera could be due to the deterioration of the egg yolk binder, which would be more sensitive than rabbit glue to the sulfation process by wet deposition of SO<sub>2</sub>. However, no chemical changes were detected on the binders. Therefore, it could be highlighted that, contrary to what happens with temperas made with other pigments exposed to the same aging test, temperas made with the selected white pigments show higher resistance to the SO<sub>2</sub> test. Finally, it would be necessary to apply more sensitive analytical techniques capable of detecting minimal changes in the organic binders to explain the slight changes in color and roughness.

**Author Contributions:** Conceptualization, T.R., J.S.P.-A. and C.C.; methodology, T.R., J.S.P.-A. and C.C.; software, J.S.P.-A.; validation, T.R., J.S.P.-A. and C.C.; formal analysis, T.R., J.S.P.-A., D.J.-D. and C.C.; investigation, T.R., J.S.P.-A., A.D. and C.C.; resources, T.R., J.S.P.-A., A.D. and C.C.; data curation, J.S.P.-A. and D.J.-D.; writing—original draft preparation, T.R., J.S.P.-A. and D.J.-D.; writing—review and editing, A.D. and C.C.; visualization, T.R. and C.C.; supervision, T.R., J.S.P.-A. and C.C.; project administration, T.R., J.S.P.-A. and C.C.; funding acquisition, T.R., J.S.P.-A. and C.C. All authors have read and agreed to the published version of the manuscript.

**Funding:** This research was funded by the Spanish Research Projects AERIMPACT (CGL2012-30729), EXPOAIR (P12-FQM-1889), LASERING-PH (PID2021-1233950A-100), the European Regional Development Fund (ERDF) and the Andalusian Research Group RNM-179.

**Data Availability Statement:** The original contributions presented in this study are included in the article. Further inquiries can be directed to the corresponding author.

**Acknowledgments:** Analyses were performed in the CACTI (*Centro de Apoyo a la Investigación*) Research Support Centre at the University of Vigo. J.S. Pozo-Antonio was supported by the RYC2020-028902-I project funded by MICIU/AEI/10.13039/501100011033 and, by “ESF Investing in your future”. Daniel Jiménez-Desmond was supported by the ED481A-2023/086 predoctoral contract through “Programa de axudas á etapa predoutoral da Xunta de Galicia” cofinanced by the European Union within the framework of the FSE+ Galicia 2021-2027 program.

**Conflicts of Interest:** The authors declare no conflicts of interest.

## References

1. La Russa, M.F.; Fermo, P.; Comite, V.; Belfiore, C.M.; Barca, D.; Cerioni, A.; De Santis, M.; Barbagallo, L.F.; Ricca, M.; Ruffolo, S.A. The Oceanus statue of the Fontana di Trevi (Rome): The analysis of black crust as a tool to investigate the urban air pollution and its impact on the stone degradation. *Sci. Total Environ.* **2017**, *593–594*, 297–309. [[CrossRef](#)] [[PubMed](#)]

2. Comite, V.; Miani, A.; Ricca, M.; La Russa, M.; Pulimeno, M.; Fermo, P. The impact of atmospheric pollution on outdoor cultural heritage: An analytic methodology for the characterization of the carbonaceous fraction in black crusts present on stone surfaces. *Environ. Res.* **2021**, *201*, 111565. [[CrossRef](#)] [[PubMed](#)]
3. Rovella, N.; Aly, N.; Comite, V.; Randazzo, L.; Fermo, P.; Barca, D.; Alvarez de Buergo, M.; La Russa, M.F. The environmental impact of air pollution on the built heritage of historic Cairo (Egypt). *Sci. Total Environ.* **2021**, *764*, 142905. [[CrossRef](#)] [[PubMed](#)]
4. Coccato, A.; Moens, L.; Vandenabeele, P. On the stability of mediaeval inorganic pigments: A literature review of the effect of climate, material selection, biological activity, analysis and conservation treatments. *Herit. Sci.* **2017**, *5*, 1–25. [[CrossRef](#)]
5. Vazquez, P.; Carrizo, L.; Thomachot-Schneider, C.; Gibeaux, S.; Alonso, F.J. Influence of surface finish and composition on the deterioration of building stones exposed to acid atmospheres. *Constr. Buil. Mater.* **2016**, *106*, 392–403. [[CrossRef](#)]
6. Herrera, A.; Cardell, C.; Pozo-Antonio, J.S.; Burgos-Cara, A.; Elert, K. Effect of proteinaceous binder on pollution-induced sulfation of lime-based tempera paints. *Prog. Org. Coat.* **2018**, *123*, 99–110. [[CrossRef](#)]
7. Naqvi, A. Decoupling trends of emissions across EU regions and the role of environmental policies. *J. Clean. Prod.* **2021**, *323*, 129130. [[CrossRef](#)]
8. Bevilacqua, N.; Borgioli, L.; Gracia, I.A. *I Pigmenti Nell'Arte Dalla Preistoria All Rivoluzi Industriale*; Il Prato: Saonara, Italy, 2003.
9. Palet, A. *Tratado de Pintura. Color, Pigmentos y Ensayo*; Edicions de la Universitat de Barcelona: Barcelona, Spain, 2002.
10. Asenjo Rubio, E. Las arquitecturas pintadas en las ciudades europeas: Aportaciones desde Málaga: La secuencia cronológica y estilística. *Boletín Arte* **2005**, *26*, 117–138. [[CrossRef](#)]
11. Ambers, J. Raman analysis of pigments from the Egyptian Old Kingdom. *J. Raman Spectrosc.* **2004**, *35*, 768–773. [[CrossRef](#)]
12. Cotte, M.; Susini, J.; Metrich, N.; Moscato, A.; Gratziu, C.; Bertagnini, A.; Pagano, M. Blackening of Pompeian Cinnabar Paintings: X-ray Microspectroscopy Analysis. *Anal. Chem.* **2006**, *78*, 7484–7492. [[CrossRef](#)]
13. Cardell, C.; Herrera, A.; Guerra, I.; Navas, N.; Rodríguez-Simón, L.; Elert, K. Pigment-size effect on the physico-chemical behavior of azurite-tempera dosimeters upon natural and accelerated photo aging. *Dyes Pigm.* **2017**, *141*, 53–65. [[CrossRef](#)]
14. Mazzeo, R.; Prati, S.; Quaranta, M.; Joseph, E.; Kendix, E.; Galeotti, M. Attenuated total reflection micro FTIR characterisation of pigment– binder interaction in reconstructed paint films. *Anal. Bioanal. Chem.* **2008**, *392*, 65–76. [[CrossRef](#)]
15. Gutman, M.; Lesar-Kikelj, M.; Mladenovič, A.; Čobal-Sedmak, V.; Križnar, A.; Kramar, S. Raman microspectroscopic analysis of pigments of the Gothic wall painting from the Dominican Monastery in Ptuj (Slovenia). *J. Raman Spectrosc.* **2014**, *45*, 1103–1109. [[CrossRef](#)]
16. Smith, G.D.; Clark, R.J. The role of H<sub>2</sub>S in pigment blackening. *J. Cult Herit.* **2002**, *3*, 101–105. [[CrossRef](#)]
17. Manzano, E.; Romero-Pastor, J.; Navas, N.; Rodríguez-Simón, L.R.; Cardell, C. A study of the interaction between rabbit glue binder and blue copper pigment under UV radiation: A spectroscopic and PCA approach. *Vib. Spectrosc.* **2010**, *53*, 260–268. [[CrossRef](#)]
18. Pozo-Antonio, J.S.; Rivas, T.; Dionísio, A.; Barral, D.; Cardell, C. Effect of a SO<sub>2</sub> Rich Atmosphere on Tempera Paint Mock-Ups. Part 1: Accelerated Aging of Smalt and Lapis Lazuli-based Paints. *Minerals* **2020**, *10*, 427. [[CrossRef](#)]
19. Pozo-Antonio, J.S.; Cardell, C.; Barral, D.; Dionísio, A.; Rivas, T. Effect of a SO<sub>2</sub> Rich Atmosphere on Tempera Paint Mock-Ups. Part 2: Accelerated Aging of Azurite-and Malachite-based Paints. *Minerals* **2020**, *10*, 424. [[CrossRef](#)]
20. Pacheco, F. *Arte de la Pintura*; Cátedra: Madrid, Spain, 1990.
21. *CIE S014-4/E:2007*; Colorimetry Part 4: CIE 1976 L\*a\*b\* Colour Space. Commission Internationale de l'éclairage. CIE Central Bureau: Vienna, Austria, 2007.
22. *UNE-EN ISO 4288:1998*; Geometrical Product Specifications (GPS)—Surface Texture: Profile Method—Rules and Procedures for the Assessment of Surface Texture. Asociación Española de Normalización y Certificación: Madrid, Spain, 1998.
23. *UNE-EN 828:2013*; Adhesives—Wettability—Determination by Measurement of Contact Angle and Surface Free Energy of Solid Surface. Asociación Española de Normalización y Certificación: Madrid, Spain, 2013.
24. Pozo-Antonio, J.S.; Barral, D.; Herrera, A.; Elert, K.; Rivas, T.; Cardell, C. Effect of tempera paint composition on their superficial physical properties- application of interferometric profilometry and hyperspectral imaging techniques. *Prog. Org. Coat.* **2018**, *117*, 56–68. [[CrossRef](#)]
25. Eastaugh, N.; Walsh, V.; Chaplin, T.; Siddall, R. *Pigment Compendium: A Dictionary of Historical Pigments*; Elsevier Butterworth-Heinemann Publications: Oxford, UK, 2007.
26. Mokrzycki, W.; Tatol, M. Color difference DeltaE-A survey. *Mach. Graph. Vis.* **2011**, *20*, 383–411.
27. Liang, H.; Keita, K.; Peric, B.; Vajzovic, T. Pigment identification with optical coherence tomography and multispectral imaging. In Proceedings of the 2nd International Topical Meeting on Optical Sensing and Artificial Vision, Saint Petersburg, Russia, 12–15 May 2008.
28. Liang, H. Advances in multispectral and hyperspectral imaging for archaeology and art conservation. *Appl. Phys. A* **2012**, *106*, 309–323. [[CrossRef](#)]

29. Nodari, L.; Ricciardi, P. Non-invasive identification of paint binders in illuminated manuscripts by ER-FTIR spectroscopy: A systematic study of the influence of different pigments on the binders' characteristic spectral features. *Herit. Sci.* **2019**, *7*, 7. [[CrossRef](#)]
30. Fuertes, S.; Laca, A.; Oulego, P.; Paredes, B.; Rendueles, M.; Díaz, M. Development and characterization of egg yolk and egg yolk fractions edible films. *Food Hydrocoll.* **2017**, *70*, 229–239. [[CrossRef](#)]
31. Pellegrini, D.; Duce, C.; Bonaduce, I.; Biagi, S.; Ghezzi, L.; Colombini, M.P.; Tinè, M.R.; Bramanti, E. Fourier transform infrared spectroscopic study of rabbit glue/inorganic pigments mixtures in fresh and aged reference paint reconstructions. *Microchem. J.* **2016**, *124*, 31–35. [[CrossRef](#)]
32. Rodríguez Blanco, J.D.; Shaw, S.; Benning, L.G. The kinetics and mechanisms of amorphous calcium carbonate (ACC) crystallization to calcite, via vaterite. *Nanoscale* **2010**, *3*, 265–271. [[CrossRef](#)] [[PubMed](#)]
33. Ji, J.; Ge, Y.; Balsam, W.; Damuth, J.E.; Chen, J. Rapid identification of dolomite using a Fourier Transform Infrared Spectrophotometer (FTIR): A fast method for identifying Heinrich events in IODP Site U1308. *Mar. Geol.* **2009**, *258*, 60–68. [[CrossRef](#)]
34. Horgnies, M.; Chen, J.J.; Bouillon, C. Overview about the use of fourier transform infrared spectroscopy to study cementitious materials. *WIT Trans. Eng. Sci.* **2013**, *77*, 251–262. [[CrossRef](#)]
35. Socrates, G. *Infrared and Raman Characteristic Group Frequencies: Tables and Charts*, 3rd ed.; John Wiley and Sons: Hoboken, NJ, USA, 2001.
36. Bishop, J.; Lane, M.; Dyar, M.; King, S.; Brown, A.; Swayze, G. What Lurks in the Martian Rocks and Soil? Investigations of Sulfates, Phosphates, and Perchlorates. Spectral properties of Ca-sulfates: Gypsum, bassanite, and anhydrite. *Am. Min.* **2014**, *99*, 2105–2115. [[CrossRef](#)]
37. Liu, Y. Raman, Mid-IR, and NIR spectroscopic study of calcium sulfates and mapping gypsum abundances in Columbus crater, Mars. *Planet. Space Sci.* **2018**, *163*, 35–41. [[CrossRef](#)]
38. Siidra, O.; Nekrasova, D.; Depmeier, W.; Chukanov, N.; Zaitsev, A.; Turner, R. Hydrocerussite-related minerals and materials: Structural principles, chemical variations and infrared spectroscopy. *Acta Crystallogr. Sect. B Struct. Sci. Cryst. Eng. Mater.* **2018**, *74*, 182–195. [[CrossRef](#)]
39. Charola, A.E.; Ware, R. Acid deposition and the deterioration of stone: A brief review of a broad topic. In *Natural Stone, Weathering Phenomena, Conservation Strategies and Case Studies*; Siegesmund, S., Weiss, T., Vollbrecht, A., Eds.; Geological Society Special Publication No. 205; The Geological Society: London, UK, 2002; pp. 393–406.
40. Cultrone, G.; Arizzi, A.; Sebastián, E.; Rodríguez-Navarro, C. Sulfation of calcitic and dolomitic lime mortars in the presence of diesel particulate matter. *Environ. Geol.* **2008**, *56*, 741–752. [[CrossRef](#)]
41. Bico, J.; Thiele, U.; Quere, D. Wetting of textured surfaces. *Colloids Surf. A Physicochem. Eng. Asp.* **2002**, *206*, 41–46. [[CrossRef](#)]

**Disclaimer/Publisher's Note:** The statements, opinions and data contained in all publications are solely those of the individual author(s) and contributor(s) and not of MDPI and/or the editor(s). MDPI and/or the editor(s) disclaim responsibility for any injury to people or property resulting from any ideas, methods, instructions or products referred to in the content.